Batteries & Supercaps

Research Article
doi.org/10.1002/batt.202200164

Chemistry Europe
European Chemical Societies Publishing

www.batteries-supercaps.org

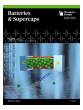

Unravelling Charge Carrier Mobility in d_0-Metal-based Spinels

Manuel Dillenz,[a] Mohsen Sotoudeh,[a] Clarissa Glaser,[c] Jürgen Janek,[c] Axel Groß,[a, b] and Holger Euchner*[b]

Enabling high Mg ion mobility, spinel-type materials are promising candidates for cathode or solid electrolyte applications. To elucidate the factors governing the observed high mobility of multivalent ions, periodic DFT calculations of various charge carriers (A = Li, Na, K, Mg, Ca, Zn and Al) in the ASc_2S_4 and ASc_2Se_4 spinel compounds were performed, resulting in the identification of a Brønsted-Evans-Polanyi-type scaling relation for the migration barriers of the various charge carriers. Combining this scaling relation with the derivation of a descriptor, solely based on easily accessible observables, constitutes a conceptual framework to investigate ion mobility in d_0-metal-based spinel chalcogenides with significantly reduced computational effort. This approach was exemplarily verified for various d_0-metal-based spinel chalcogenide compounds AB_2X_4 (B = Sc, Y, Ga, In, Er and Tm; X = O, S and Se) and led to the identification of d_0-metal-based CaB_2O_4 spinels as promising compounds possibly enabling high Ca ion mobility.

Introduction

Multivalent batteries represent interesting alternatives to the state-of-the-art lithium-ion battery technology and may contribute to meet the growing demand for high energy and low-cost energy storage systems. Increased safety, beneficial environmental aspects as well as high volumetric energy densities, are some of the promising prospects.[1,2] Especially, the possible use of metal anodes, substantiated by the low tendency for dendrite formation in multivalent ion batteries,[3–6] constitutes a promising advantage. Currently, the most advanced multivalent battery technology is based on magnesium, however, electrolyte stability, high partial electronic conductivity of reported Mg solid electrolytes (SEs), the lack of high voltage cathodes as well as problems with the sluggish Mg^{2+} kinetics still constitute challenges that need to be overcome. Concerning the desired cathode properties, spinel-type phases are a highly interesting class of materials. In fact, oxide spinels show high insertion voltages but the so far investigated compounds are plagued by sluggish kinetics of the extraction/insertion reactions of multivalent ions such as Mg^{2+}, Ca^{2+} or Zn^{2+}.[7–9] However, the ion mobility and therefore the kinetics can be improved by moving towards sulfide and selenide-based spinels instead.[10] Here, increasing the size and the polarizability of the anion described by the electronegativity facilitates the charge redistribution and rehybridization along the migration path of the charge carrier, thus leading to reduced migration barriers.[11,12] On the downside, the improved ion mobility is connected with reduced insertion potentials which translates into a rather low energy density of selenide spinel cathodes.

Nevertheless, selenide spinels are interesting compounds for applications as solid electrolyte in solid-state batteries. A promising candidate for it's use as solid electrolyte is $MgSc_2Se_4$, showing low migration barriers of $E_{mig} = 0.370 \pm 90$ meV.[10] However, the use as solid electrolyte is hindered by substantial partial electronic conductivity[13] that is ~0.04% of the ionic conductivity.[10] Based on the reported experimental data for $MgSc_2Se_4$,[10] we calculated for a charged $Mg|MgSc_2Se_4|Mo_6S_8$ battery with an assumed cell voltage of 2 V a non-negligible self-discharge current of 0.43 µA across a separator with 6 mm diameter. We estimate that a loss of 10% can be expected after just 16 hours (see Supporting Information). In order to decrease its relatively high self-discharge rate, the electronic conductivity of the solid electrolyte has to be minimized. Here, strategies to reduce electronic conductivity such as aliovalent doping or variation of the synthesis conditions – leaving the high ionic conductivity untouched – may help to overcome these issues.[14,15] Previously, we have investigated the mobility of various charge carriers in a $MgSc_2Se_4$-based model system by theoretical means,[12] providing valuable insights on the role of the ionic size, charge, and bonding character of the investigated charge carriers in the spinel structure. Furthermore, we recently showed that the respective stability of ions with octahedral and tetrahedral coordination environment that is

[a] M. Dillenz, Dr. M. Sotoudeh, Prof. Dr. A. Groß
Institute of Theoretical Chemistry, Ulm University, Albert-Einstein-Allee 11, 89081 Ulm, Germany
[b] Prof. Dr. A. Groß, Dr. H. Euchner
Helmholtz Institute Ulm (HIU) for Electrochemical Energy Storage, Helmholtzstraße 11, 89081 Ulm, Germany
E-mail: holger.euchner@uni-tuebingen.de
[c] C. Glaser, Prof. Dr. J. Janek
Institute of Physical Chemistry & Center for Materials Research (ZfM/LaMa), Justus Liebig University, Heinrich-Buff-Ring 17, 35392 Giessen, Germany

Supporting information for this article is available on the WWW under https://doi.org/10.1002/batt.202200164

Research Article
doi.org/10.1002/batt.202200164
Chemistry Europe
European Chemical Societies Publishing

described by the site preference in chalcogenide spinels can only be understood if deviations from a purely ionic interaction are taken into account.[16] Therefore, we have introduced the squared electronegativity difference of the charge carrier and the anion $\Delta\chi^2_{A-X}$ in order to characterize the non-ionic components of the interaction that contribute to the bonding. Following this concept, we proposed a design principle based on $\Delta\chi^2_{A-X}$ to improve the ion mobility in crystalline solids.[17]

Here, we have extended our computational investigation of the charge carrier migration barriers to a variety of ASc_2S_4 and ASc_2Se_4 spinel compounds (with A = Li, Na, K, Mg, Ca, Zn and Al). A Brønsted-Evans-Polanyi-type linear scaling relation[18] of the activation energy and the site preference of the charge carriers is observed, allowing to propose a descriptor for the migration energies in spinel-type materials. These findings were exemplarily verified for various d_0-metal-based spinel chalcogenide compounds of AB_2X_4 stoichiometry (B = Sc, Y, Ga, In, Er and Tm; X = O, S and Se).

Results and Discussion

Compounds adopting the spinel structure show the characteristic AB_2X_4 stochiometry and usually crystallize in the space group $Fd\bar{3}m$ (see Figure 1(a)). Spinel compounds relevant for the use in batteries commonly consist of a charge carrier A, a transition metal B and a chalcogenide X (X = O, S or Se). The chalcogenide anions form a face-centered cubic lattice with the A cations occupying one-eighth of the tetrahedral AX_4 interstices and the B cations residing in half of the octahedral BX_6 interstices. Due to the crystal field effect, the covalent interaction splits the five degenerate *d*-orbitals of the octahedrally coordinated TM cation into three low-lying t_{2g}-orbitals and two high-lying e_g-orbitals. In the spinel structure, the *d*-orbitals covalently interact with the anion *p*-orbitals forming σ- and π-bonding, while A cations like Mg primarily interact ionically. However, a deviation from the ionic picture for A cations such as Mg is necessary to get a proper understanding of the site preference. Compounds like $MgSc_2X_4$ obviously do not contain electrons in the *d*-orbitals, with the resulting density of states (DOS) consequently showing empty *d*-orbitals as conduction band, as exemplified for the case of $MgSc_2S_4$ (see Figure 1(c)).

Charge carrier migration in the spinel structure proceeds through a three-dimensional network of empty octahedra which act as channels for the charge carriers (see Figure 1(b)). The migration path connects two tetrahedral sites via an octahedral site (tet-oct-tet) while the triangular face, connecting the tetrahedron and octahedron, typically constitutes the transition state of the migration. Since the migration path is symmetric, only the migration from tetrahedral to octahedral site has to be calculated and the results can simply be mirrored.

Migration pathways for the charge carrier spinels ASc_2Se_4 and ASc_2S_4, as obtained via the Nudged Elastic Band (NEB) method (see computational details), are shown in Figure 2 and may be compared to previous results on the diffusion of the A charge carrier in a $MgSc_2Se_4$ spinel model system with a fixed $Mg_{0.875}A_{0.125}Sc_2Se_4$ geometry.[12] While the overall trend remains similar, the barrier heights are drastically reduced in the fully relaxed systems presented here. Interestingly, for the charge carrier Zn, the site preference for the tetrahedral site is so strongly pronounced that the transition state coincides with the octahedral site, as compared to the other charge carriers where the triangular face constitutes the transition state of the ion migration. Comparing the NEB calculated migration barriers of a given charge carrier A in the respective sulfide and selenide spinels (see Figure 2(a) and (b)), reveals two main trends. First, the transition state energy seems to be of comparable size in the sulfide and selenide compounds for most charge carriers. Furthermore, the results indicate that the octahedral site is somewhat stabilized relative to the tetrahedral site in the selenides as compared to the sulfides. As already mentioned, the tet-oct-tet energy profile of the migration path

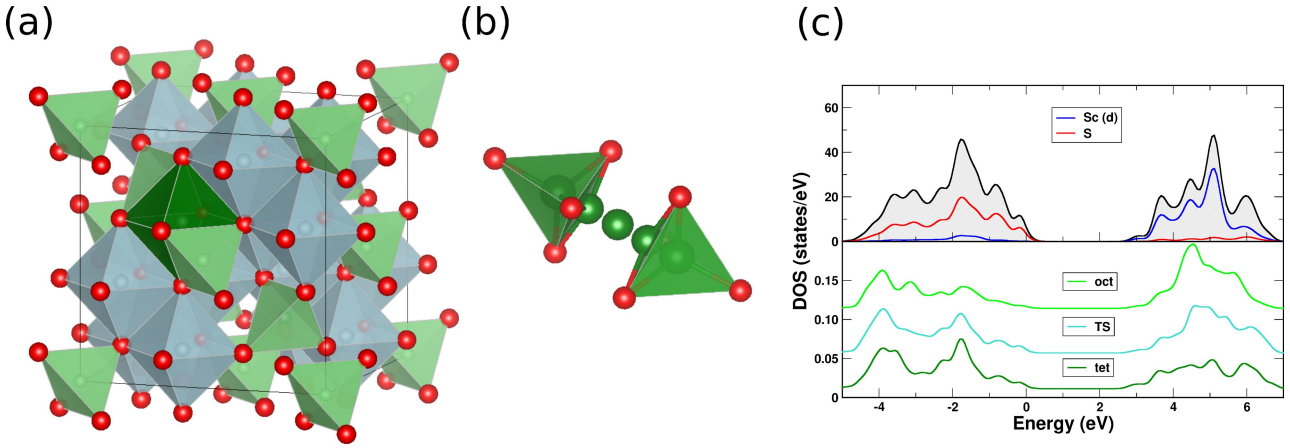

Figure 1. (a) The AB_2X_4 spinel structure. The X anions (red) form a face-centered cubic lattice, the B cations (blue) are octahedrally coordinated, and the A cations (green) occupy tetrahedrally coordinated sites. A possible intermediate state is indicated in dark green. (b) The schematic representation of a diffusion path between two adjacent tetrahedral sites (tet-oct-tet) (c) The density of states (DOS) of $MgSc_2S_4$ and the corresponding local density of states (LDOS) of the charge carrier in tetrahedral, octahedral and transition state (TS) coordination.

Research Article
doi.org/10.1002/batt.202200164
Chemistry Europe
European Chemical Societies Publishing

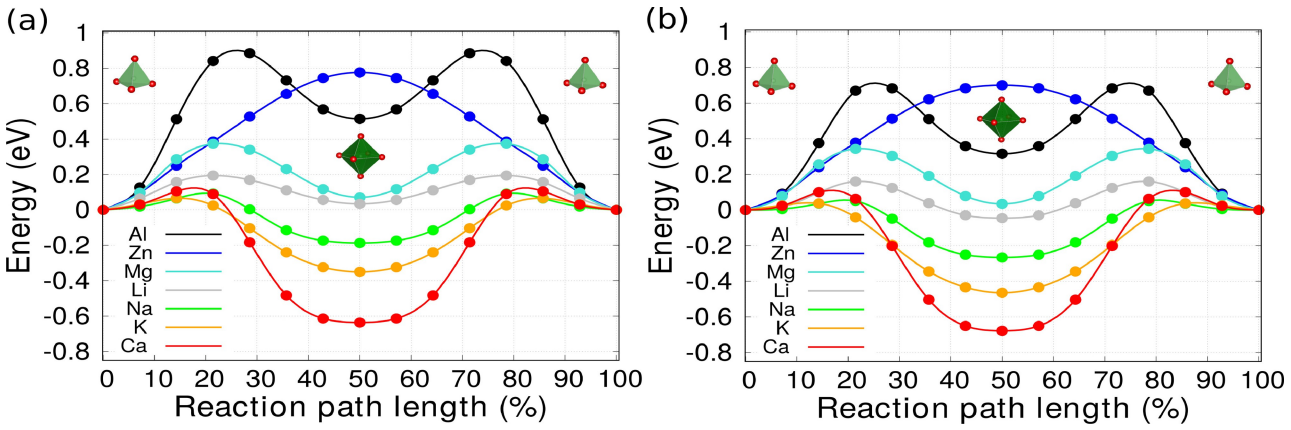

Figure 2. The tet-oct-tet migration pathways of the charge carrier A in (a) ASc_2S_4 and (b) ASc_2Se_4. Energies along the migration path are presented relative to the energy of the charge carrier in tetrahedral coordination.

of the charge carriers may be decomposed into a migration from the initial tetrahedral to the intermediate octahedral site and a corresponding symmetric migration from the intermediate octahedral to the final tetrahedral site (see Figure 1).

As discussed previously,[12] the charge carrier migration barrier between the tetrahedral and octahedral site of the spinel structure may be interpreted as resulting from a combination of two contributions. For most spinel compounds the difference in energy between the tetrahedral and octahedral site, generally referred to as the site preference,[19] contributes significantly to the overall migration barrier. This energy difference may then be expressed as a static contribution to the migration barrier. Furthermore, the transition state influences the migration barrier as well, which thus can be understood as a kinetic contribution.

To separate these kinetic contributions from the often dominant static part of the overall migration barrier, kinetically resolved activation barriers E_{KRA} have been calculated (see Equation 1). Moreover, the introduction of kinetically resolved activation barriers[20] cures the direction dependence of the migration barriers:

$$E_{KRA} = E_{TS} - \frac{1}{2}(E_{oct} - E_{tet}). \quad (1)$$

Interestingly, Li^+ and Na^+ show very similar E_{KRA} barriers, both for the respective sulfide and selenide spinels, as Table 1 demonstrates. Furthermore, the bivalent charge carriers also show very similar E_{KRA} values for sulfide and selenide spinels alike. Comparing the kinetically resolved barriers for the monovalent Li^+ and Na^+ ions with those of the bivalent charge carriers Mg^{2+}, Ca^{2+} and Zn^{2+} reveals that the bivalent charge carriers show a E_{KRA} value approximately twice as high as those for the monovalent charge carriers. This observed correlation of the kinetically resolved activation barrier with the valence of the charge carrier n_A can simply be expressed as

$$E_{KRA,A} = n_A \times E_{KRA,Li}, \quad (2)$$

Table 1. Migration barriers E_{NEB} and kinetically resolved activation barriers E_{KRA} for the ASc_2S/Se_4 compounds. The migration barrier E_{NEB} is the difference in energy of the energetic minimum (octahedral or tetrahedral) and the energetic maximum (TS) along the migration path coordinate.

Charge carrier A	$E_{NEB,S}$ [eV]	$E_{KRA,S}$ [eV]	$E_{NEB,Se}$ [eV]	$E_{KRA,Se}$ [eV]
Li	0.19	0.18	0.21	0.18
Na	0.28	0.19	0.32	0.18
K	0.42	0.24	0.50	0.27
Mg	0.37	0.34	0.34	0.33
Ca	0.74	0.38	0.78	0.44
Zn	0.78	0.39	0.70	0.35
Al	0.88	0.63	0.68	0.53

with $E_{KRA,Li} = 0.18$ eV being the kinetically resolved activation barrier of Li^+ in the hypothetical compounds $LiSc_2S_4$ and $LiSc_2Se_4$. Now, the total migration barrier can be estimated by only determining the site preference of the charge carrier $\Delta E = E_{oct} - E_{tet}$, resulting in the following expression, which takes the form of a Brønsted-Evans-Polanyi-type relation (see discussion below):

$$E_{BEP,A} = n_A \times E_{KRA,Li} + \frac{1}{2}|\Delta E|. \quad (3)$$

In Figure 3, the approximated migration barriers (E_{BEP}) are compared with the corresponding migration barriers obtained from the NEB calculations (E_{NEB}). The E_{BEP} barriers agree very well with the E_{NEB} barriers in the case of the ASc_2S_4 compounds while showing slightly larger deviations in the case of the selenide spinels. The fact that the ion charge n_A explicitly enters the scaling relation in Equation 3 points towards the importance of the ion charge for the transition state energy E_{TS}. The ion size, on the other hand, strongly influences the site preference and hence implicitly affects the static second term in Equation 3. Interestingly, Equation 3 indicates that minimizing the energy difference between tetrahedral and octahedral site, i.e. reducing the site preference ΔE, of the charge carrier A, might be a valid strategy to improve the ion mobility in spinel-type phases. Tuning the site preference to values close to zero, the overall migration barrier would be approximately

Research Article
doi.org/10.1002/batt.202200164
Chemistry Europe
European Chemical Societies Publishing

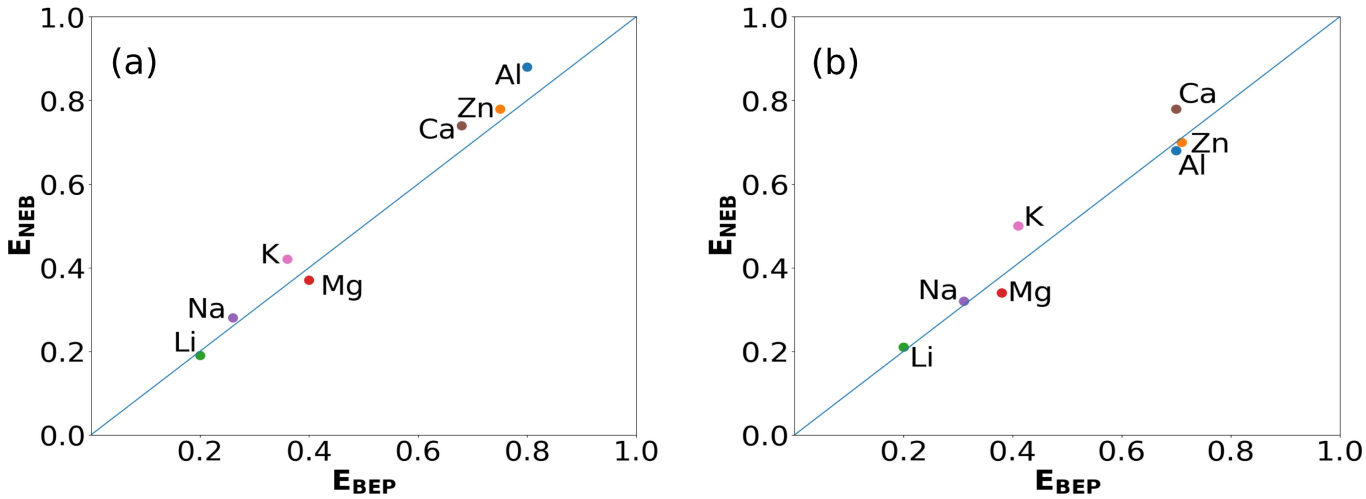

Figure 3. Migration barriers E_{NEB} obtained from NEB calculations plotted as a function of the barriers E_{BEP} predicted from the BEP relation Equation 3 for (a) ASc_2S_4 and (b) ASc_2Se_4 spinels.

determined by $E_{mig}(\Delta E \approx 0) = n_A \times E_{KRA,Li}$, therefore proposing lower limits for the migration barriers, amounting to $E_{mig} = 0.18$ eV for monovalent and $E_{mig} = 0.36$ eV for bivalent charge carriers, respectively.

Notably, the presented scaling relation strongly resembles the Brønsted-Evans-Polanyi-type[21,22] relations observed in heterogeneous catalysis.[23–26] In general, the Brønsted-Evans-Polanyi (BEP) relation is based on the observation that often there is a linear relationship between the activation energy and the reaction energy for an elementary reaction. In heterogeneous catalysis, the BEP relation provides a method for estimating activation barriers from adsorption energies, by assuming the linear relationship between the activation barrier for dissociation E_a and the stability of the adsorbed intermediates on the surface ΔE_{ads}, characterized by the respective adsorption energy. The scaling relation presented here represents a similar linear relationship of the activation energy of migration E_{mig} and the stability of the intermediate octahedral site relative to the tetrahedral site, characterized by the site preference ΔE, for charge carriers of the same valency n_A. Furthermore, Equation 3 is a fast way to estimate the migration energy in spinel-type materials, since computationally demanding NEB calculations can be substituted by the much cheaper calculations of the site preference.

Note that in the BEP relation Equation 3, the energy difference $\Delta E = E_{oct} - E_{tet}$ between the tetrahedral and the octahedral site serves as a descriptor for the migration barrier in d_0-spinels which still needs to be computed. We now like to go a step further and address the question whether ΔE can be estimated from some materials parameters in a reasonable way. In a recent work,[16] k_{64} – the ratio of the Mg–X bond length in octahedral (d_6) and tetrahedral (d_4) coordination – has been found to allow for a qualitative prediction of the site preference in spinel type materials.

To find a quantitative descriptor for the site preference ΔE, we have combined DFT calculations of total energies with a machine learning approach. For the identification of the relevant quantities entering a descriptor, we applied a statistical compressed-sensing approach using the sure-independence screening and sparsifying operator SISSO.[27] In order to find the best descriptor, we used a two-step approach. First, we have chosen the so-called primary features which correspond to materials properties that might be relevant for the site preference. We have selected the following features: The formal oxidation states of the cations and the anions (n_A, n_X), the electronegativity of A cations (χ_A) and X anions (χ_X), the ionic radii of A cations (r_A) and X anions (r_X), A–X bond lengths in threefold (d_3), fourfold (d_4), and sixfold coordination (d_6), and an electrostatic potential term, described by the inverse of the bond lengths ($V_i = i/d_i$).

In this first step, using SISSO[27] we identified the main features to enter a potential descriptor, namely the square of the electronegativity difference $\Delta\chi^2$, the oxidation state of the cation n_A, as well as the sum of the ionic radii of the charge carrier cation and the anion ($r_X + r_A$) in the octahedral sites d_6. Interestingly, the parameters that are found to determine the site preference agree well with those in a recently proposed general descriptor[17] for the migration barriers in crystalline solids, defined as the product of bond radius, oxidation states and deviation from the ionic picture, described by the square of the electronegativity difference $\Delta\chi^2$. Note that all these materials parameters are easily available, i.e., no additional calculations are required to obtain these input values. In a second step, we restricted the initial features in the machine-learning approach to those just mentioned above to obtain a more suited descriptor. Thus we obtained the following descriptor for the dimensionality $\Omega = 1$,

$$D = \frac{scd(\Delta\chi^2)}{(r_A + r_X)n_A}, \tag{4}$$

with a rather satisfactory total root mean square error (RMSE) of only 0.02. Here, $\Delta\chi^2$ enters in the form of a standard Cauchy distribution

Research Article
doi.org/10.1002/batt.202200164
Chemistry Europe
European Chemical Societies Publishing

$$scd(\Delta\chi^2) = \frac{1}{\pi(1+(\Delta\chi^2)^2)}. \quad (5)$$

Despite the still remaining complexity of D, the computed dependencies using the SISSO reveal the important factors that influence the site preference. In particular, the difference in electronegativity of the anion and the charge carrier $\Delta\chi_{A-X}$ strongly contributes to quantify the energy difference between the octahedral and tetrahedral sites. Note that the descriptor does not directly correspond to the site preference energy. However, these two quantities are connected by a linear relationship that has to be determined by least-square fitting.

Figure 4 illustrates the reliability of combining the descriptor for the site preference (Equation 4) and the BEP-like scaling relation for the migration barrier (Equation 3). For any given system, we first estimated the site preference ΔE using the descriptor given in Equation 4 (panels (b) and (d)) and then we plugged these values into the BEP-like scaling relations to determine the migration barriers E_{BEP}. Panels (a) and (c) compare these predicted barriers with the barriers E_{NEB} determined from DFT calculations using the NEB method. The NEB calculated barriers are in rather good agreement with the migration barriers obtained in this two-step descriptor approach for both the sulfides ((a)) and the selenides ((c)). The values of the proposed descriptor for the sulfide and selenide spinels are given on the x-axes in Figure 4(b) and (d). For a given charge carrier they differ only slightly since the differences in the ionic radii of the S^{2-}- and the Se^{2-}-ions and in the respective electronegativities of S and Se partly cancel each other in the calculation of the descriptor.

In order to verify the presented framework of scaling relation and descriptor, we applied it to other sulfide and selenide spinels. The results for the Y-, In- and Tm-based sulfide and selenide spinels are shown in Figure 5. Overall, the combination of site preference descriptor and empirical scaling relation yields good agreement with the NEB calculations. Interestingly enough, this approach does not only yield good results for the d_0-metals Sc and Y, but also for the non-d_0-metals Ga, In, Er and Tm. The results for these compounds that are not included in Figure 5 are provided in Figure S1 of the supporting information. We attribute this to the fact that non-

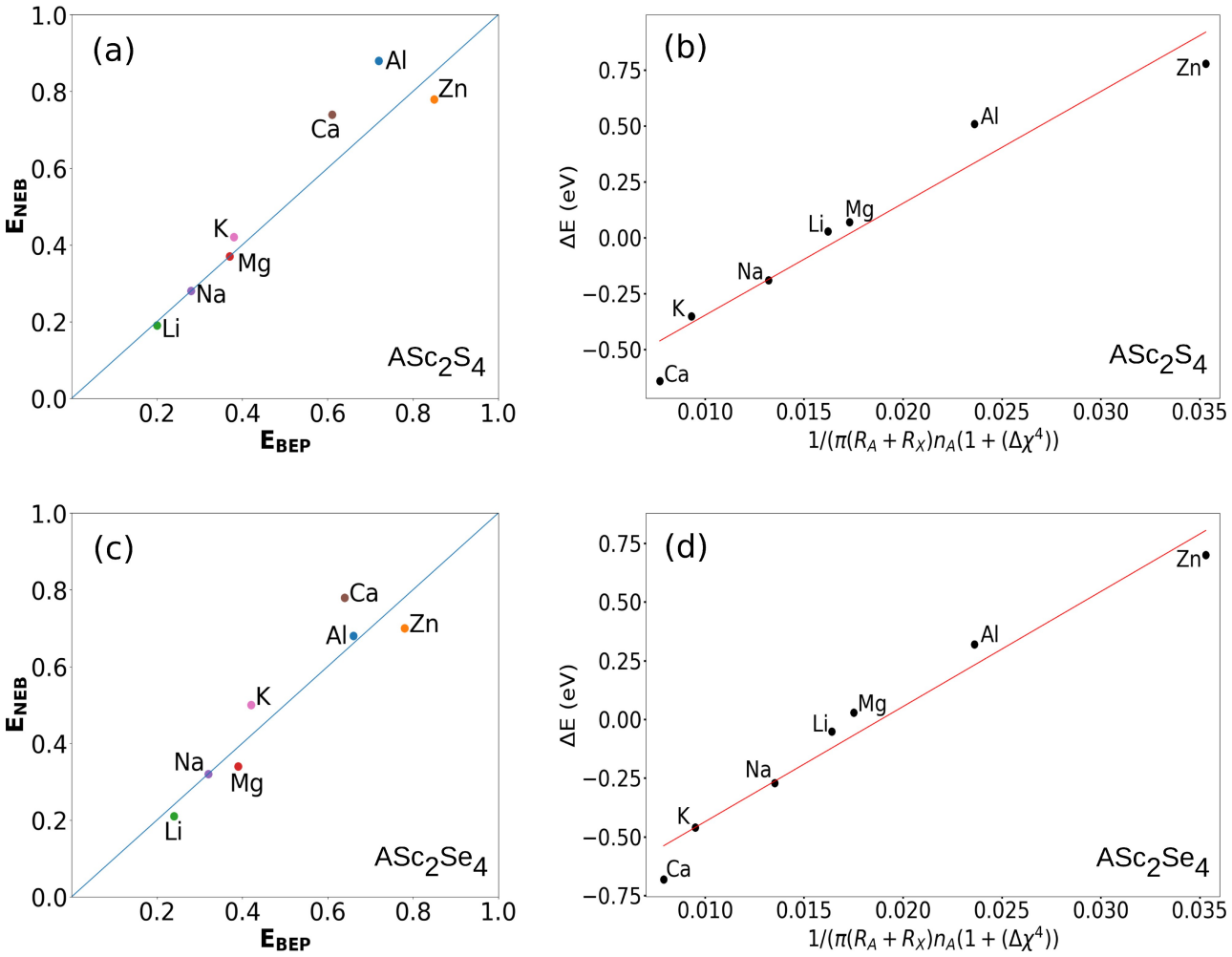

Figure 4. The approximated migration barriers E_{BEP} using the site preference descriptor for ΔE are plotted against the migration barriers obtained from NEB calculations E_{NEB} for the (a) ASc_2S_4 and the (c) ASc_2Se_4 spinels. Additionally, the fits of the descriptor for the site preference ΔE for the (b) ASc_2S_4 and the (d) ASc_2Se_4 spinels are shown.

Research Article
doi.org/10.1002/batt.202200164
Chemistry Europe
European Chemical Societies Publishing

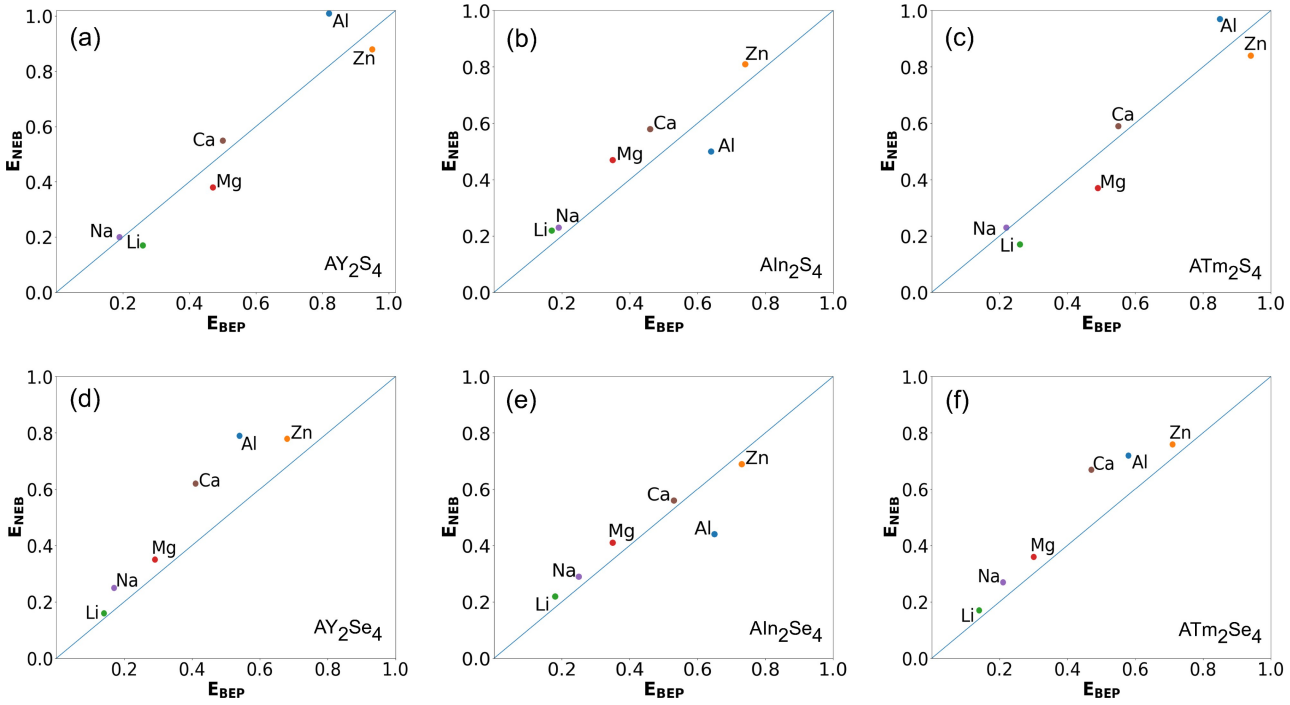

Figure 5. The approximated migration barriers E_{BEP} are plotted against the migration barriers obtained from NEB calculations E_{NEB} for the exemplary set of sulfide and selenide spinels (a) AY_2S_4, (b) AIn_2S_4, (c) ATm_2S_4, (d) AY_2Se_4, (e) AIn_2Se_4 and (f) ATm_2Se_4.

d_0-metal-based spinels are structurally very similar to d_0-metal spinels, both do for example not exhibit significant distortions of the coordination polyhedra.

While the framework was derived solely based on the results for the Sc-based sulfide and selenide spinels, we checked whether its predictions are also valid for d_0-metal-based oxide spinels. In Figure 6, we compare predicted BEP barriers for barrier heights below 1 eV for Sc- and In-based oxide spinels to the barriers obtained by DFT-NEB calculations. Due to the high migration barriers of more than 1 eV, the results for Al are not included in Figure 6. Further oxide spinel compounds are consideredin Figure S1 of the supporting information. Again, we obtain a good agreement between predicted and calculated barriers, demonstrating the wide applicability of our approach.

After having established the validity of our two-step predictor approach, we also like to comment on the significance of the calculated barrier heights for the ion mobility in electrode and solid electrolyte materials. In general, our results indicate that many oxide, sulfide, and selenide spinels with empty *d*-orbitals may offer high ionic mobility for Li, Na, Mg, and Ca with migration barriers below 0.5 eV – provided that the pre-factor of the mobility shows no unexpected anomaly. In order to identify further materials with low migration barriers, the approach developed by us may be used for fast exploration of the chemical space of d_0-metal-based spinel chalcogenides for the charge carriers A = Li, Na, Mg, Ca, Zn and Al. As mentioned above, Equation 3 suggests, that high ion mobility may be achieved by tuning the site preference towards small values. Moreover, detailed considerations of the

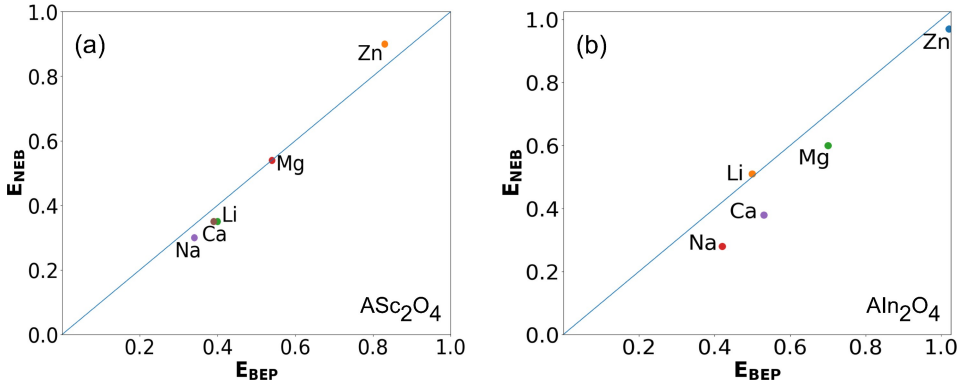

Figure 6. The approximated migration barriers E_{BEP} are plotted against the migration barriers obtained from NEB calculations E_{NEB} in the range from $0 - 1$ *eV* for the exemplary set of d_0-metal based spinel oxides (a) ASc_2O_4 and (b) AIn_2O_4.

Research Article
doi.org/10.1002/batt.202200164
Chemistry Europe
European Chemical Societies Publishing

different quantities entering Equation 3 reveal two possible strategies to lower the activation energy of ion migration in the spinel structure: 1) Finding superionic Li-ion conductors to reduce $E_{KRA,Li}$; 2) Minimizing the energy difference between tetrahedral and octahedral sites to reduce the site preference.

While the valency of the ion is determined by the chosen chemistry, Equation 3 suggests, that finding superionic Li-ion conductors constitutes a way to minimize $E_{KRA,Li}$, and thus, the kinetic contributions to the overall migration barrier. Following Sotoudeh et al.,[17] minimizing $E_{KRA,Li}$ may be achieved by choosing the constituent elements of the host lattice in such a way that the electronegativity difference between the migrating cations and the anions of the host lattice is reduced.

On the other hand, the migration barrier can also be dominated by the static contribution related to the difference in the site preference of the charge carriers. Thus, special emphasis should actually be denoted to optimizing the static contribution. Indeed our calculations suggest, that the previously reported high Mg ion mobility in certain spinel compounds[9,10,13,15,28,29] stems from the fact, that the site preference ΔE of the Mg ion is very low (e.g. $\Delta E_{MgSc_2S_4} = 0.03$ eV). Similarly, the calculated high migration barriers of the corresponding Zn–Sc and Ca–Sc sulfide compounds can be explained by the calculated high site preferences of $\Delta E_{ZnSc_2S_4} = 0.7$ eV and $\Delta E_{CaSc_2S_4} = -0.68$ eV, respectively. Thus, to design spinel compounds with increased Zn or Ca ion mobility, a reduction of the respective site preferences needs to be achieved. Since the transition state energy, and thus, the kinetically resolved activation barrier E_{KRA} are expected to be similar for all bivalent ions (see Equation 3), tuning the corresponding site preference may lead to similarly high ion mobility for the Zn and Ca ions, as for the case of the Mg ion. In fact, the results for the CaB_2O_4 (B = Sc, In) spinel compounds that have been presented in Figure 6, indicate that oxide spinels with increased Ca mobility may exist.

In these oxide spinels, the tetrahedral site is stabilized relative to the octahedral site resulting in low site preferences and thus, in small migration barriers $E_{mig} < 0.5$ eV. The corresponding NEB results, additionally including results for Y-, Ga-, Tm- and Er-based spinel oxides are depicted in Figure 7(a). These very low Ca migration barriers are of similar size as the observed low Mg ion migration barriers in selenide-based and some sulfide-based spinels (see Figure 5).

Notably, the low migration barriers in oxide spinels suggest, that high Ca ion mobility in the spinel structure does not necessarily require highly polarizable anions like S^{2-} and Se^{2-}. This observation in combination with Equation 3 suggests, that the high Mg ion mobility observed experimentally in the spinel structure (more specifically in $MgSc_2Se_4$) mainly originates from changes in ΔE and not from the influence of the polarizability of the anion on the transition state energy. Consequently, these results also indicate that high Mg ion mobility in oxide spinels could be implemented by tuning the site preference, possibly resulting in spinel compounds with advantages concerning sustainability and chemical properties.

Finally, the previously discussed importance of the site preference ΔE can nicely be illustrated by plotting the DFT calculated migration barriers E_{NEB} against the site preference ΔE for the various investigated charge carriers. Indeed, the distribution of the migration barriers shows the expected minimum at $\Delta E = 0$ eV, illustrating the dominant contribution of ΔE to the overall migration barrier and thus emphasizing the importance of minimizing the site preference as a design criterion for high ion mobility in the spinel structure.

While the here presented approach is tailormade for d_0-metal-based spinel chalcogenides, and therefore does not include redox-active transition metals, it offers a framework that may easily be extended. A modification of the scaling relation and the descriptor framework to account for the influence of *d*-electron containing TMs – typically resulting in distorted spinel structures – will allow to investigate a

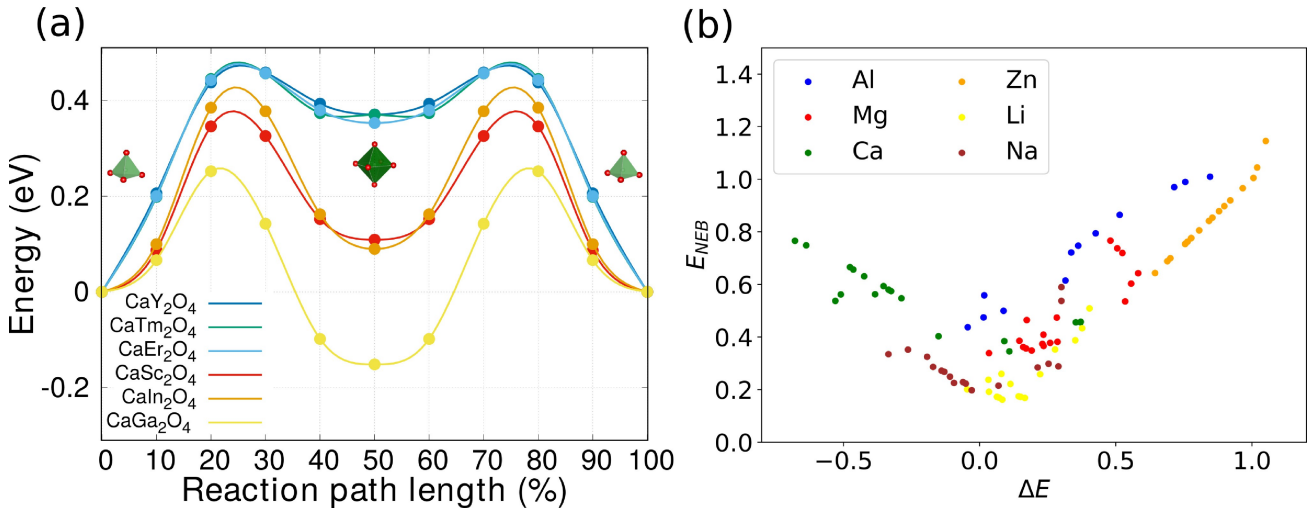

Figure 7. (a) The tet-oct-tet migration of the charge carrier Ca in CaB_2O_4 with B = Sc, Y, Ga, In, Er and Tm. The energies are depicted relative to the energy of the charge carrier in tetrahedral coordination. (b) The migration barriers obtained from NEB calculations E_{NEB} plotted against the site preference ΔE for the Al- (blue), Mg- (red), Ca- (green), Zn- (orange), Li- (yellow) and Na-based (brown) compounds.

Research Article
doi.org/10.1002/batt.202200164

significantly increased chemical space. Extending the framework, however, will most likely require to include additional parameters that account for the impact of the distortion in non-d_0-type spinels (here the anion parameter u may be a suited candidate).

Furthermore, the here presented scaling relation may be transferred to other structure types showing migration pathways passing at least two (meta-)stable insertion sites allowing the identification of kinetically resolved activation barriers for migration. This is in fact a frequently occurring scenario, which the application of the descriptor might probably only need certain adaptions for.

Conclusion

Applying periodic DFT calculations, we have studied the migration barriers for jumps of various charge carriers A (A = Li, Na, Mg, Ca, Zn and Al) in ASc_2S_4 and ASc_2Se_4 spinel compounds. Based on kinetically resolved activation barriers E_{KRA} and the site preference ΔE of the charge carrier in the respective coordination environment, we introduced a Brønsted-Evans-Polanyi-type scaling relation in combination with a descriptor for ΔE. The descriptor, was obtained by a statistical compressed-sensing approach and the important factors entering the descriptor were verified, using the sure-independence screening and sparsifying operator SISSO.[27] The derived framework of scaling relation and descriptor was verified on a variety of d_0-metal-based spinel chalcogenides.

While low Mg ion activation barriers in several d_0-metal-based spinel chalcogenides were previously predicted in theoretical studies and high mobility was shown in one case experimentally,[10,12,13,15,28] the here presented combination of a BEP-type scaling relation with a descriptor for the crucial parameter of the site preference offers a framework to systematically explore the chemical space of d_0-metal-based spinel chalcogenides for the investigated charge carriers. Applying the presented framework, allowed to identify candidate materials with potentially high theoretical Ca ion mobility, such as d_0-metal-based CaB_2O_4 spinels. While this study is limited to the investigation of the ion migration barriers, it has to be noted, that other important aspects apart from a potentially resulting high ion mobility need to be fulfilled for the application in battery cathodes or solid electrolytes. Since d_0-metal-based spinel chalcogenides combine a redox-inactive d_0-metal and chalcogenide anions, the class of d_0-metal-based spinel chalcogenides may be limited to the application as solid-electrolyte materials. Further possible prohibiting effects may be limited phase stability in the spinel structure, the degree of inversion or anti-site defects causing electronic conductivity in the material.

Moreover, the presented approach constitutes a framework that may be extended to redox-active 3*d* and 4*d* transition metals, by capturing electronic and geometrical effects induced by the partially populated *d*-orbitals.[16,30]

In general, the here presented approach provides a conceptual framework to systematically explore the migration barriers of various charge carriers in spinel chalcogenides with drastically reduced computational effort. Identifying the factors that determine the migration barriers, moreover, improves our understanding of ion mobility in solids. Furthermore, applying the descriptor will allow to make predictions for electrode and solid electrolyte materials with improved ion mobility and thus guide the design of superior materials for electrochemical energy storage applications.

Computational Details

First-principles calculations

Periodic density functional theory (DFT)[31,32] calculations were performed to study the ion migration barriers in ASc_2X_4 (A = Li, Na, K, Mg, Ca, Zn and Al; X = S and Se) compounds. Exchange and correlation are accounted for by the Perdew-Burke-Ernzerhof (PBE) generalized gradient approximation.[33] The electron-core interactions are represented by the Projector Augmented Wave[34] method as implemented in the Vienna *Ab initio* Simulation Package.[35–37] Charge neutral calculations were performed using the conventional 56 atom cubic unit cell of the spinel structure and the Brillouin zone was sampled using a 2×2×2 k-point grid. The electronic structure was converged within 1×10^{-6} eV, applying a plane-wave cutoff energy of 520 eV. The inital and final geometries for the ion migration were obtained by converging all forces on the atoms within 0.01 eV Å^{-1}. The migration barriers were obtained by the climbing image Nudged Elastic Band (NEB) method for the low vacancy limit, corresponding to one vacancy per supercell. All NEB calculations were performed using four distinct images while all forces on the atoms were converged within 0.05 eV Å^{-1}. A minimum distance of more than 10 Å between periodic images was ensured.[38]

Machine-learning approach

In our search for a suitable descriptor for the site preference – the relative stability of octahedral vs. tetrahedral site – we have applied a statistical compressed-sensing approach using the sure-independence screening and sparsifying operator SISSO.[27] In this approach, the first step is the selection of the so-called primary features (ϕ_0) – elementary material properties like e.g. bond length or ionic radii.

Then a feature space is constructed by using the initial primary features and combining them by different mathematical operations (in our case 13 operations have been selected). The same construction scheme is then applied for the creation of the subsequent feature spaces, until a final candidate feature space (consisting of the features ϕ_n) is reached. Important (highly correlated) features in this feature space are then identified by sure independence screening and linear combinations thereof are subsequently applied to determine a suitable descriptor for the desired quantity – in our case the energy difference between tetrahedral and octahedral site. For this work, the rung of the feature space to be constructed was set to n = 3 and the dimension of the descriptor to Ω = 1 A linear relationship between descriptor and site preference energy is finally obtained for the here investigated system by using a minimization procedure based on the sparsifying operator (SO).

Acknowledgements

Financial support from the Cluster of Excellence POLiS (EXC-2154, project ID 390874152) of the Deutsche Forschungsgemeinschaft (DFG) and Computer time provided by the state of Baden-Württemberg through bwHPC and the German Research Foundation (DFG) through grant no INST 40/575-1 FUGG (JUSTUS 2 cluster) are gratefully acknowledged. This work contributes to the research performed at CELEST (Center for Electrochemical Energy Storage Ulm-Karlsruhe). Open Access funding enabled and organized by Projekt DEAL.

Conflict of Interest

The authors declare no conflict of interest.

Data Availability Statement

The data that support the findings of this study are available on NOMAD under the following DOI https://dx.doi.org/10.17172/NOMAD/2021.11.18-1 and from the corresponding author upon reasonable request.

Keywords: descriptor · ion mobility · scaling relation · solid electrolyte · spinel

[1] G. A. Elia, K. Marquardt, K. Hoeppner, S. Fantini, R. Lin, E. Knipping, W. Peters, J.-F. Drillet, S. Passerini, R. Hahn, *Adv. Mater.* **2016**, *28*, 7564–7579.
[2] F. Maroni, S. Dongmo, C. Gauckler, M. Marinaro, M. Wolfahrt-Mehrens, *Batteries & Supercaps* **2021**.
[3] D. Aurbach, Y. Cohen, M. Moshkovich, *Electrochem. Solid-State Lett.* **2001**, *4*, A113.
[4] M. Matsui, *J. Power Sources* **2011**, *196*, 7048–7055.
[5] M. Jäckle, K. Helmbrecht, M. Smits, D. Stottmeister, A. Groß, *Energy Environ. Sci.* **2018**, *11*, 3400–3407.
[6] D. Stottmeister, A. Groß, *ChemSusChem* **2020**, *13*, 3147–3153.
[7] M. Mao, T. Gao, S. Hou, C. Wang, *Chem. Soc. Rev.* **2018**, *47*, 8804–8841.
[8] M. Liu, Z. Rong, R. Malik, P. Canepa, A. Jain, G. Ceder, K. A. Persson, *Energy Environ. Sci.* **2015**, *8*, 964–974.
[9] Z. Rong, R. Malik, P. Canepa, G. Sai Gautam, M. Liu, A. Jain, K. Persson, G. Ceder, *Chem. Mater.* **2015**, *27*, 6016–6021, .
[10] P. Canepa, S.-H. Bo, G. S. Gautam, B. Key, W. D. Richards, T. Shi, Y. Tian, Y. Wang, J. Li, G. Ceder, *Nat. Commun.* **2017**, *8*, 1–8.
[11] E. Levi, M. Levi, O. Chasid, D. Aurbach, *J. Electroceram.* **2009**, *22*, 13–19.
[12] M. Dillenz, M. Sotoudeh, H. Euchner, A. Groß, *Front. Energy Res.* **2020**, *8*, 260.
[13] L.-P. Wang, Z. Zhao-Karger, F. Klein, J. Chable, T. Braun, A. R. Schür, C.-R. Wang, Y.-G. Guo, M. Fichtner, *ChemSusChem* **2019**, *12*, 2286–2293.
[14] P. Canepa, G. Sai Gautam, D. Broberg, S.-H. Bo, G. Ceder, *Chem. Mater.* **2017**, *29*, 9657–9667.
[15] S. Kundu, N. Solomatin, Y. Kauffmann, A. Kraytsberg, Y. Ein-Eli, *Appl. Mater. Res.* **2021**, *23*, 100998.
[16] M. Sotoudeh, M. Dillenz, A. Groß, *Adv. Energy Sustain. Res.* **2021**, *2*, 2100113.
[17] M. Sotoudeh, A. Groß, *JACS Au* **2022**, *2*, 463–471.
[18] T. Bligaard, J. K. Nørskov, S. Dahl, J. Matthiesen, C. H. Christensen, J. Sehested, *J. Catal.* **2004**, *224*, 206–217.
[19] S. K. Kolli, A. Van der Ven, *ACS Appl. Energ. Mater.* **2018**, *1*, 6833–6839.
[20] A. Van der Ven, G. Ceder, M. Asta, P. D. Tepesch, *Phys. Rev. B* **2001**, *64*, 184307.
[21] J. Bronsted, *Chem. Rev.* **1928**, *5*, 231–338.
[22] M. Evans, M. Polanyi, *Trans. Faraday Soc.* **1938**, *34*, 11–24.
[23] V. Pallassana, M. Neurock, *J. Catal.* **2000**, *191*, 301–317.
[24] A. Logadottir, T. H. Rod, J. K. Nørskov, B. Hammer, S. Dahl, C. Jacobsen, *J. Catal.* **2001**, *197*, 229–231.
[25] Z.-P. Liu, P. Hu, *J. Chem. Phys.* **2001**, *114*, 8244–8247.
[26] J. K. Nørskov, T. Bligaard, A. Logadottir, S. Bahn, L. B. Hansen, M. Bollinger, H. Bengaard, B. Hammer, Z. Sljivancanin, M. Mavrikakis, *et al., J. Catal.* **2002**, *209*, 275–278.
[27] R. Ouyang, S. Curtarolo, E. Ahmetcik, M. Scheffler, L. M. Ghiringhelli, *Phys. Rev. Mater.* **2018**, *2*, 083802.
[28] M. Liu, A. Jain, Z. Rong, X. Qu, P. Canepa, R. Malik, G. Ceder, K. A. Persson, *Energy Environ. Sci.* **2016**, *9*, 3201–3209.
[29] J. Koettgen, C. J. Bartel, G. Ceder, *Chem. Commun.* **2020**, *56*, 1952–1955.
[30] K. E. Sickafus, J. M. Wills, N. W. Grimes, *J. Am. Ceram. Soc.* **1999**, *82*, 3279–3292.
[31] P. Hohenberg, W. Kohn, *Phys. Rev.* **1964**, *136*, B864–B871.
[32] W. Kohn, L. J. Sham, *Phys. Rev.* **1965**, *140*, A1133–A1138.
[33] J. P. Perdew, K. Burke, M. Ernzerhof, *Phys. Rev. Lett.* **1996**, *77*, 3865–3868.
[34] P. E. Blöchl, *Phys. Rev. B* **1994**, *50*, 17953–17979.
[35] G. Kresse, J. Hafner, *Phys. Rev. B* **1993**, *47*, 558–561, Jan .
[36] G. Kresse, J. Furthmüller, *Phys. Rev. B* **1996**, *54*, 11169–11186.
[37] G. Kresse, D. Joubert, *Phys. Rev. B* **1999**, *59*, 1758–1775.
[38] D. Sheppard, R. Terrell, G. Henkelman, *J. Chem. Phys.* **2008**, *128*, 134106.

Manuscript received: April 5, 2022
Accepted manuscript online: April 12, 2022
Version of record online: June 1, 2022